nature nanotechnology

NOVEMBER 2009 VOL 4 NO 11
www.nature.com/naturenanotechnology

Single-crystal nanobeams take the strain

NANOFLUIDICS
Off the wall

IMAGING AGENTS
Going beneath the skin

PHASE-CHANGE MEMORY
Under pressure

LETTERS
PUBLISHED ONLINE: 13 SEPTEMBER 2009 | DOI: 10.1038/NNANO.2009.266
nature nanotechnology

Strain engineering and one-dimensional organization of metal–insulator domains in single-crystal vanadium dioxide beams

J. Cao[1,2], E. Ertekin[3], V. Srinivasan[3], W. Fan[1,4], S. Huang[1], H. Zheng[2,5], J. W. L. Yim[1,2], D. R. Khanal[1,2], D. F. Ogletree[2,6], J. C. Grossman[3] and J. Wu[1,2,3]*

Correlated electron materials can undergo a variety of phase transitions, including superconductivity, the metal–insulator transition and colossal magnetoresistance[1]. Moreover, multiple physical phases or domains with dimensions of nanometres to micrometres can coexist in these materials at temperatures where a pure phase is expected[2]. Making use of the properties of correlated electron materials in device applications will require the ability to control domain structures and phase transitions in these materials. Lattice strain has been shown to cause the coexistence of metallic and insulating phases in the Mott insulator VO_2. Here, we show that we can nucleate and manipulate ordered arrays of metallic and insulating domains along single-crystal beams of VO_2 by continuously tuning the strain over a wide range of values. The Mott transition between a low-temperature insulating phase and a high-temperature metallic phase usually occurs at 341 K in VO_2, but the active control of strain allows us to reduce this transition temperature to room temperature. In addition to device applications, the ability to control the phase structure of VO_2 with strain could lead to a deeper understanding of the correlated electron materials in general.

Lattice strain, if tuned continuously, would be a sensitive means to shed light on the origin of phase inhomogeneity. In contrast to conventional materials, where elastic deformation causes continuous, minor variations in material properties, lattice strain has a profound influence on the electrical, optical and magnetic properties of correlated electron materials (CEMs) through coupling between the charge, spin and orbital degrees of freedom of electrons[3]. If phase inhomogeneity is absent in strain-free, single-crystal specimens, but can be introduced and modulated by external strain, it would then be possible to eliminate or strain engineer the inhomogeneity and domains in CEMs for nanoscale device applications. Previous strain studies of CEMs have been limited to epitaxial thin films. Biaxial strain imposed from lattice mismatch with the substrate has been shown to enhance remarkably the order parameters in ferroelectric[4–6] and high-T_C superconducting epilayers[7]. In these films the lattice-mismatch strain distribution is complicated by misfit dislocations. In contrast, free-standing, single-crystal CEM nanostructures are dislocation-free, and can be subjected to coherent and continuously tunable external stress. CEM phase transitions and domain dynamics can then be explored through *in situ* microscopic experiments varying strain and temperature independently. Such an approach would enable, for the first time, probing of CEMs at the single domain level under continuous tuning of their lattice degree of freedom.

VO_2 is a CEM that, in the strain-free state, undergoes a first-order metal–insulator phase transition (MIT) at $T_C^0 = 341$ K with a change in conductivity of several orders of magnitude. The MIT is accompanied by a structural phase transition from the high-temperature tetragonal phase (metallic, M) to the low-temperature monoclinic phase (insulating, I). On cooling through the MIT, the vanadium ions dimerize and these pairs tilt with respect to the tetragonal *c*-axis, causing the specimen to expand by $\varepsilon_0 \approx 1\%$ along the *c*-axis[8–10]. Along the tetragonal *a*- and *b*-axes, on the other hand, the lattice shrinks by 0.6 and 0.1%, respectively, causing a volume expansion of 0.3% (refs 8–10). The relationship between the MIT and the accompanying structural transition in VO_2 has been a topic of debate for decades[11–13]. As expected from the abrupt change in lattice constant with the phase transition, a uniaxial compressive (tensile) stress along the tetragonal *c*-axis direction would drive the system towards the M (I) phase. In the stress–temperature phase diagram, the rate at which the transition temperature T_C is modified by the uniaxial stress σ is given by the Clausius–Clapeyron equation,

$$dT_C/d\sigma = (\varepsilon_0 T_C^0)/\Delta H \quad (1)$$

where ΔH is the latent heat of the transition. $dT_C/d\sigma$ was measured to be $\sim$1.2 K kbar^{-1} for *c*-axis uniaxial stress[14]. As the volume change at the MIT is much weaker than the *c*-axis expansion, it is expected from the Clausius–Clapeyron equation that T_C is much more sensitive to uniaxial stress than to hydrostatic pressure. This offers an efficient way to organize M–I domains in single-crystal VO_2 by imposing a uniaxial strain distribution. It has been shown that single-crystal VO_2 nanobeams fully clamped on a SiO_2 surface spontaneously exhibit periodic M–I domains near T_C^0 owing to uniaxial strain imposed by elastic mismatch with the substrate[15,16]. The work was recently advanced by etching the fully clamped system into an end-clamped configuration, and interesting phase coexisting phenomena were observed[17]. In the present work, instead of passively observing the strain effect, we fully eliminate the substrate-imposed strain and then induce and continuously modulate the MIT by artificially stressing the VO_2. Single-crystal VO_2 micro- and nanobeams were prepared with the length direction along the tetragonal *c*-axis (see Methods). We established coherent strain fields in the VO_2 beams by bending or applying uniaxial stress. The small width and the single-crystal nature of these beams

[1]Department of Materials Science and Engineering, University of California, Berkeley, California 94720, USA, [2]Materials Sciences Division, Lawrence Berkeley National Laboratory, Berkeley, California 94720, USA, [3]Berkeley Nanosciences and Nanoengineering Institute, University of California, Berkeley, California 94720, USA, [4]Department of Thermal Science and Energy Engineering, University of Science and Technology of China, Hefei, China, [5]National Centre for Electron Microscopy, Lawrence Berkeley National Laboratory, Berkeley, California 94720, USA, [6]Molecular Foundry, Lawrence Berkeley National Laboratory, Berkeley, California 94720, USA. *e-mail: wuj@berkeley.edu

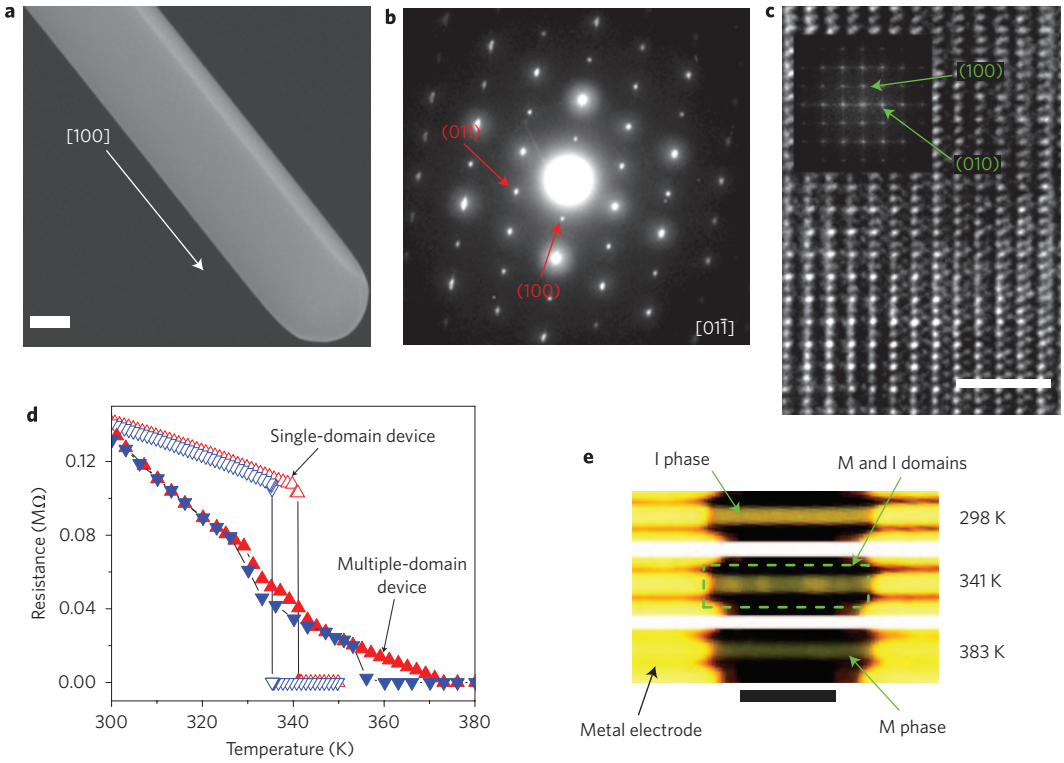

Figure 1 | Structural and electrical characterization of VO_2 beams. a, Scanning electron microscope image of a VO_2 beam grown along the monoclinic [100] direction (tetragonal *c*-axis) showing the facet surface. **b**, Selected area electron diffraction pattern for a 100-nm-wide nanobeam indexed using a [01$\bar{1}$] zone axis. **c**, High-resolution transmission electron microscope image of a VO_2 nanobeam. The inset shows the corresponding fast Fourier transform pattern indexed to monoclinic VO_2 with a [001] zone axis. **d**, Resistance of VO_2 beams measured in four-probe geometry as a function of temperature. The free-standing VO_2 beam shows single-domain behaviour (open triangles: red, heating; blue, cooling), whereas the clamped VO_2 beam shows multiple domains during the transition (filled triangles). **e**, Optical images of the multiple-domain device taken at different temperatures. The top (298 K) and bottom (383 K) images show the pure insulating and metallic phases, respectively. The middle image (341 K) shows the coexistence of metallic and insulating domains in the device. Scale bars, 100 nm (**a**), 2 nm (**c**), and 5 μm (**e**).

allowed them to withstand an extraordinarily high uniaxial strain (>2.5%, as compared to <1% in bulk) without plastic deformation or fracture. The system responded to the strain field by self-organizing one-dimensionally micro- to nanoscale M–I domains along the beam length. Such an active and continuous control of the phase inhomogeneity opens possibilities for device applications of the MIT in VO_2. We generated a strain–temperature phase diagram for VO_2, and demonstrated the MIT in VO_2 at room temperature for the first time.

Figure 1a–c shows low- and high-resolution images of typical VO_2 beams. By adjusting the synthesis conditions, the beams can be grown with either a weakly coupled beam–substrate interface that slips to relieve stress, or a strongly coupled, clamped interface that pins the beam to the substrate. In the latter case thermal stress is imposed on the beams after cooling from the growth temperature to room temperature. Both types of beams were incorporated into four-probe devices using lithography. With increasing temperature, devices made from the unstressed beams displayed a sharp drop of resistance at $T_C^0 = 341$ K (Fig. 1d, single-domain device). When heated through the transition temperature, the beam shows an abrupt change in brightness in white-light optical microscope images, from bright reflection in the low-temperature I phase to dark reflection in the high-temperature M phase. In contrast, the electrical resistance of the clamped beams decreases gradually across a wide phase-transition temperature range, showing an effective second-order phase transition. High-magnification optical imaging of the clamped beams revealed multiple M and I domains appearing during the transition, where dark domains nucleated in the bright phase and grew with increasing temperature, finally merging into a single M phase. A direct correlation between optical contrast and the electronic phases is therefore established, where bright and dark reflection indicates the I and M phase, respectively.

Clamped VO_2 beams of various widths (300 nm to 5 μm) displayed periodic M–I domains in high-resolution optical microscopy within the transition range (see Supplementary Information). Such a periodic domain pattern forms spontaneously as a result of the competition between strain energy in the elastically mismatched VO_2/substrate system and domain wall energy in the VO_2 (ref. 16). The period of the pattern is determined by the balance between the strain-energy minimization that favours small, alternating M–I domains and domain-wall energy minimization that opposes them[16,18]. The domain structure could not be resolved by optical microscopy on beams narrower than 300 nm, and beams wider than 5 μm displayed an irregular, two-dimensional domain texture, possibly due to biaxial or non-uniform strain (as in the case of thin films). We focused our optical study on beams with widths between 1 and 2 μm, in which the micro-domains could be readily imaged and the local strain was easily controlled. In these beams a chain of M–I domains self-organize along the beam axis with a characteristic domain size comparable to the beam width.

To establish a wider range of coherent strain in the VO_2 beam, we bent non-clamped beams on the substrate by pushing part of the beam with a microprobe. A large compressive (tensile) strain results near the inner (outer) edge of the high-curvature regions of the bent beam. Figure 2a shows the development of an array of triangular domains along a bent VO_2 beam imaged at different temperatures. The bent beam was in I phase at room temperature.

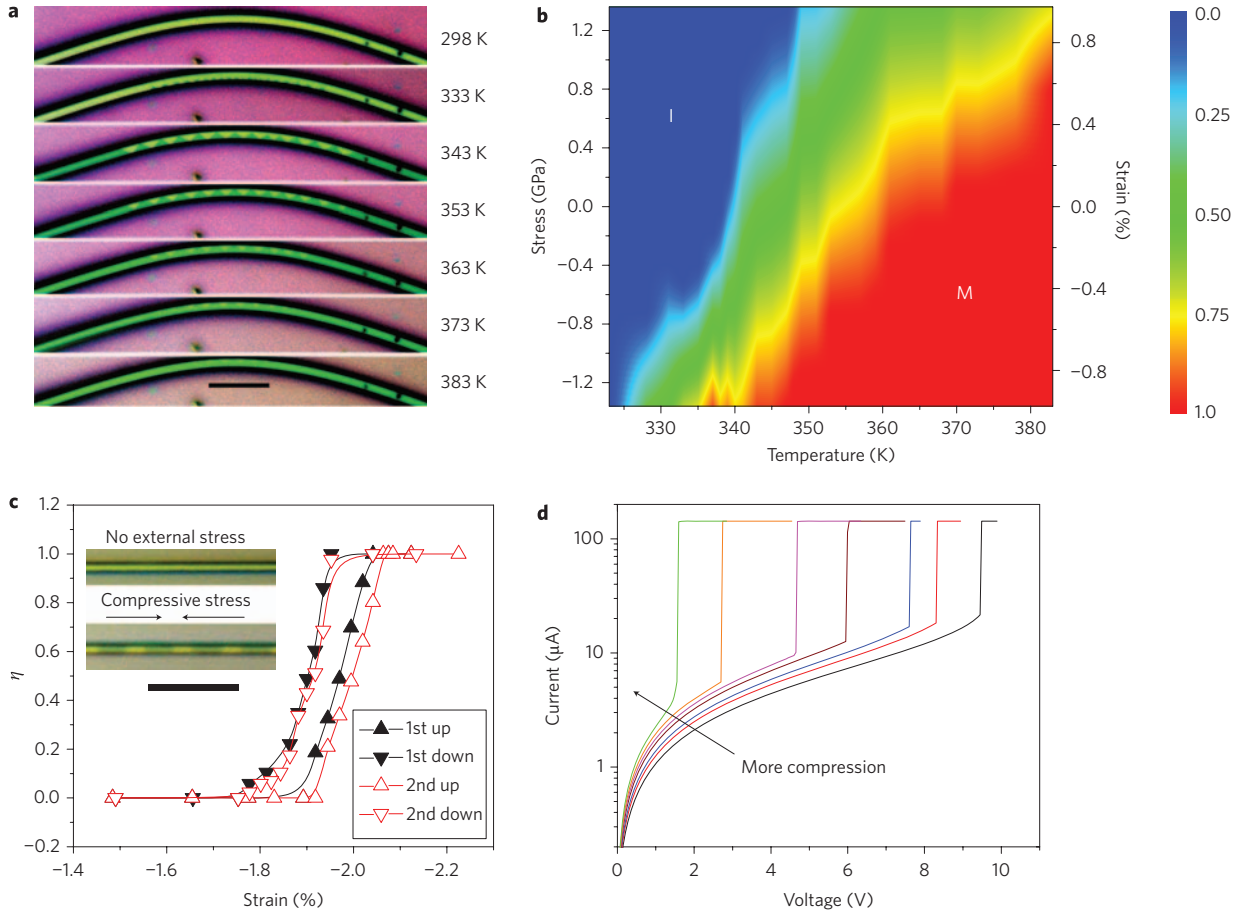

Figure 2 | Strain-induced metal–insulator transitions along VO_2 beams. a, Optical images of an array of triangular metallic (M, dark regions) and insulating (I, bright regions) domains nucleated and co-stabilized by tensile and compressive strain during heating. A colour-inverted image with better contrast between the I and M phases is included in the Supplementary Information. **b**, Phase diagram showing the fraction of the M phase (red is 100% M and blue is 100% I; see colour bar) as a function of temperature (*x*-axis) and uniaxial stress (*y*-axis, left) or strain (*y*-axis, right). Data were extracted by optical measurements from the bent beam shown in **a. c**, Uniaxial compression reversibly induces a metal–insulator transition (MIT) at room temperature in clamped VO_2 beams. The inset shows representative optical images of M–I domains along a stressed beam. **d**, Room-temperature *I–V* characteristic of a VO_2 beam under different axial compressions, showing a MIT induced by Joule heating, with the threshold voltage and current both being significantly reduced by the external compression. The experiment was carried out under ambient conditions. Scale bars in **a** and **c**, 10 μm.

At elevated temperatures, sub-micrometre, periodic triangular M domains started to nucleate at the inner edge of the bent region where the strain was the most compressive. These domains continued to grow and expand with increasing temperature, while the triangular geometry and periodic arrangement were maintained. At $T \approx T_C^0 = 341$ K, the straight, strain-free part of the beam switched abruptly to the M phase as expected, while the bent part of the beam showed a nearly 50%–50% coexistence of M and I domains. These domains were highly periodic and triangular, with each triangle running through the entire width of the beam. As temperature was further increased, the M phase expanded toward the outer edge and finally completely eliminated the I phase at $T \approx 383$ K. Upon cooling (not shown), the domain evolution was reversed, with a $\sim$10 *K* hysteresis from the heating process. Therefore, the domain organization at the microscale evolves from a periodic, nanoscale phase nucleation.

To quantitatively understand the strain-stabilized M–I phase coexistence, the bent part of the beam is approximated with a constant curvature geometry in which the strain varies linearly from compression to tension in the radial direction across a neutral plane. Assuming an equal Young's modulus for both the M and I phases ($Y = 140$ GPa; ref. 19), the stress is calculated from $\sigma = Y\varepsilon$ along the radial direction. The optically determined M-phase fraction η, at each radius, was measured from Fig. 2a and plotted in $\sigma - T_C$ phase space in Fig. 2b. As expected, the system was in pure M phase ($\eta = 1$) at high temperatures and high compressive stresses, and in pure I phase ($\eta = 0$) at low temperatures and high tensile stresses. At intermediate temperatures and stresses, M and I phases coexisted with the spatial arrangement and relative fraction determined by energy minimization. According to equation (1), the boundary separating the M and I phases in the $\sigma - T_C$ phase diagram in Fig. 2b is directly related to the latent heat of the MIT. Fitting the experimental data using the upper and lower boundaries, we obtain a latent heat of ΔH between 1,200 and 950 cal mol^{-1}. This value is consistent with a ΔH of 1,025 cal mol^{-1} reported for bulk VO_2 (refs 20,21). Note that these values are nearly four times higher than the latent heat calculated from the $\sigma - T_C$ data reported recently[17]. This difference might be because the phase transition in ref. 17 is between another monoclinic phase (M_2) and the rutile M phase.

Assuming a linear M–I phase boundary, the $\sigma - T_C$ phase diagram predicts that a compressive strain of $\sim$2.2% would be sufficient to drive VO_2 from I to M phase at room temperature. To test this prediction, we applied compressive stress directly along the length of a VO_2 beam clamped onto a soft substrate[22] and investigated how η changed with external stress (see Methods). With increasing compressive

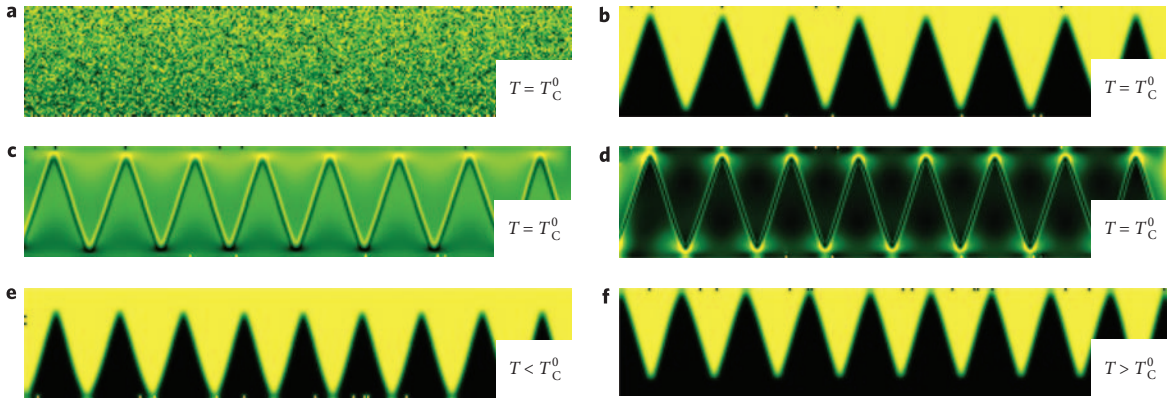

Figure 3 | Phase field modelling of domain formation in a bent VO_2 beam. a, At first, the metallic (M, dark green) and insulating (I, yellow) phases are randomly distributed at the natural MIT temperature, T_C^0. **b**, Equilibrium phase distribution showing a self-organized array of M and I phases at T_C^0. **c**, Equilibrium strain (ε_{xx}) distribution at T_C^0: yellow and dark green denote the maximum tensile and maximum compressive strain, respectively. **d**, Equilibrium strain energy density distribution: yellow denotes the highest strain energy density; dark green denotes the lowest. **e**,**f**, Equilibrium phase distribution showing more of the I phase (yellow) at a temperature below T_C^0 (**e**), and more of the M phase (dark green) above T_C^0 (**f**).

stress along the beam axis, periodic M phase (dark domains) emerged out of the I phase (bright part) and gradually expanded, eventually merging to form a pure M phase beam. The VO_2 beam was monitored optically and η was measured as a function of the total strain. As shown in Fig. 2c, the beam remained entirely insulating ($\eta = 0$) until stressed to a total strain of $\varepsilon \approx -1.9\%$, then entered a strain regime where periodic M and I domains coexisted, ultimately reaching a full M state ($\eta = 1$) at $\varepsilon \approx -2.1\%$. Upon releasing the strain from the M state, the η–ε curve showed a hysteretic behaviour and the beam returned to a full I state at $\varepsilon \approx -1.8\%$.

As the resistance of the VO_2 beams changes by several orders of magnitude across the MIT, this actively controlled, room-temperature phase transition can be used as a 'strain-Mott' transistor. Very recently, Joule heating-induced MIT in single VO_2 nanowires was used to achieve a novel type of gas sensor[23]. The nanowire was self-heated into the M phase when the bias voltage exceeded a threshold (V_{th}). The sensitivity and selectivity to different pressures and species of gas molecules came from their different thermal conductivity to dissipate the Joule heat away from the nanowire. However, a large V_{th}, thus a high operation power, was typically needed to achieve such device function[23]. The strain sensitivity of the MIT provides a strategy to drastically reduce the operation power and hence potentially increase the sensitivity and lifetime of these devices. In Fig. 2d we show such an effect observed from a self-heated VO_2 device under uniaxial compression at room temperature. Over the range of compression, V_{th} and threshold current were reduced by a factor of 5 to 6; consequently, the operation power was reduced by a factor of 30. Further compression directly drove the device to the M state without the need for Joule heating, which can be seen from the trend of decreasing resistance of the I phase at $V < V_{th}$. Active and extensive control of strain in these nano/microbeams thus offers a new 'knob' to tune the MIT for novel or improved device applications.

To understand if the domain patterns self-organized along the beams are to be expected given the material parameters of VO_2 and the geometric dimensions of the beams, we implemented a two-dimensional phase field model, where the total energy $F(\phi)$ is equal to the sum of bulk thermodynamic energy, interfacial (domain wall) energy and strain energy,

$$F(\phi) = \int \left[f(\phi) + \frac{\beta^2}{2}|\nabla\phi|^2 + \frac{1}{2}C_{ijkl}(\varepsilon_{ij} - \varepsilon_{ij}^{T})(\varepsilon_{kl} - \varepsilon_{kl}^{T}) \right] \mathrm{d}A \quad (2)$$

The parameter ϕ denotes the phase, where $\phi = 0$ corresponds to M and $\phi = 1$ corresponds to I. A double well potential $f(\phi)$ describes the relative thermodynamic energy of the M and I phases and is temperature dependent. The second term reflects the interfacial energy. The last term is the elastic energy, where C is the elastic modulus tensor, ε the strain, and ε^T the lattice mismatch between the two phases: ε_{xx}^T varies smoothly from $\varepsilon_0 = 0$ to 1% as the phase varies from $\phi = 0$ to 1, and ε_{yy}^T and ε_{xy}^T are 0. The parameters used in the modelling are typical for bulk VO_2 (refs 16,19). In the simulations, the phase distribution evolves from an initial random phase distribution (Fig. 3a) according to Cahn–Allen dynamics under boundary conditions corresponding to a uniform beam bending. Videos showing the evolution of the phases and the accompanying relaxation of the strain field are available in the Supplementary Information.

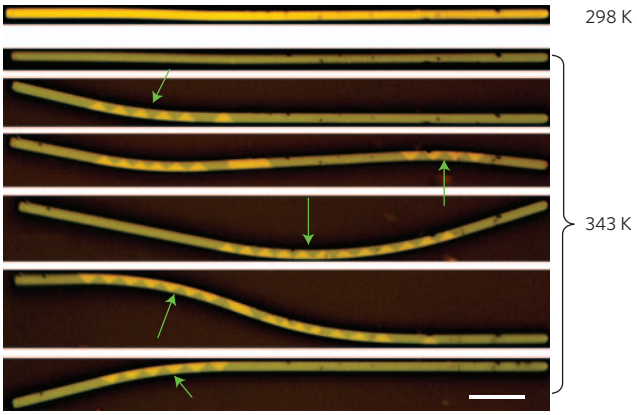

Figure 4 | Strain engineering domains in a VO_2 beam. Before bending, the beam was purely insulating (bright, top image) at 298 K and purely metallic (dark, second image) at 343 K. A tungsten needle (denoted by the arrows) was used to push-bend the beam, which created I domain arrays in the strained regions. Scale bar, 10 μm.

At $T = T_C^0$, the equilibrium phase distribution shows a periodic, triangular domain pattern as shown in Fig. 3b, demonstrating quantitatively that realistic geometric, elastic and interfacial energy parameters give rise to the patterns observed in the experiment. This pattern nearly completely relieves the strain energy in the bent beam, with some remnant strain at the triangular tips (Fig. 3c). Between the upper and lower edges, the ratio of metal and insulator phases varies linearly for optimal strain energy relief, corresponding exactly to the initial linear variation of strain. The period varies for different interfacial energy density and

elastic constants. Specifically, the period is determined by competing effects of strain energy relaxation and interfacial energy minimization: a smaller period results in more effective strain energy relief, but at the cost of introducing more interfacial area. This effect is commonly observed in, for instance, spinodally decomposing systems in which strain stabilizes periodic microstructures[24]. Finally, we illustrate in Fig. 3 the equilibrium phase distributions for systems that are slightly below or above T_C^0, which also agree well with the experimental observation in Fig. 2a.

It is intriguing to compare the coexistence of M and I phases in the VO_2 beams to the phase inhomogeneity observed in CEM thin films, such as Mott insulators[25], colossal magnetoresistive manganites[2,26–32] and high-T_C superconductors[33]. Specifically in VO_2, an M–I phase coexistence within a range near T_C^0 in polycrystalline VO_2 films grown on Al_2O_3 substrates was recently observed using scanning near-field infrared microscopy[25]. Upon heating across T_C^0 the M phase grows out of the I phase in a random, percolative manner, with the size of M and I domains ranging from the nano- to microscale. In contrast, in our single-crystal VO_2 beams, not surprisingly, the M and I phases coexist and evolve from the nano- to microscale in an orderly fashion in response to the continuous tuning of coherent strain.

The sensitivity of the electronic phases to local strain allows one to manipulate and engineer the functional domains through external stress. Figure 4 shows various domain patterns stabilized in one VO_2 beam by bending different parts of the beam. Initially the beam was strain-free, and therefore in pure I phase at room temperature and pure M phase at 343 K. When the beam was locally bent at 343 K, an array of triangular I domains were created in the high curvature region in response to the local tensile strain. These domains were highly mobile and could be driven to different locations along the beam by slight modifications of the bending geometry. Strain manipulation of M–I domains along a VO_2 beam was recorded as a video (see Supplementary Information). In all cases, the spatial inhomogeneity and arrangement of the M and I phases could be understood from the total energy minimization of the system. The active control of the phase transition by strain offers a new approach to directly probe sub-domain behaviour of VO_2 in uncharted phase space such as the M_2 phase[8].

In summary, uniaxial external stress was used to engineer M–I domains along single-crystal beams of VO_2, and to observe the Mott M–I transition at room temperature. The ability to engineer phase inhomogeneity and phase transitions with strain opens opportunities for designing and controlling functional domains of VO_2 for device and sensor applications. As distinctly different physical and chemical properties are associated with these phases, interfacing strain-engineered VO_2 with other molecular, nano- or polymeric materials may provide new assembly strategies to achieve collective and externally tunable functionalities.

Methods

Single-crystalline VO_2 beams were grown using a vapour transport method reported previously (see Supplementary Information) and characterized using scanning electron microscopy (SEM), transmission electron microscopy (TEM) and selected area electron diffraction[16,34]. These VO_2 beams grow along the tetragonal *c*-axis with {110} planes as the bounding side faces[34]. The width of these beams varies from 50 nm to a few micrometres and their length ranges from tens to a few hundred micrometres. In the experiment of applying compressive stress to single VO_2 beams, single-crystal VO_2 beams (typical length ~100 μm, width ~0.5–2 μm) were transferred to a polycarbonate or Kapton substrate (thickness ~1 mm). A set of metal contacts were patterned using lithography and deposited using sputtering (15 nm chromium and 400 nm gold) for electromechanical measurements. Epoxy was used to bury and bond the VO_2 beam onto the substrate, and cured immediately at 390 K for 30 min. This step ensured that the VO_2 beam was clamped onto the substrate when it was in M phase, and therefore when the VO_2 was cooled down to I phase at room temperature, a spontaneous compressive strain of $\varepsilon_0 \approx 1\%$ (due to the MIT) and another compressive strain of ~0.4% (due to thermal expansion mismatch with the polycarbonate substrate) were frozen in the system. By three-point concave bending of the polycarbonate or Kapton substrate along the length direction of the VO_2 beam, further uniaxial compressive stress was added to the VO_2 beam. A strain gauge was glued in the centre of the substrate and used to monitor the additional strain imposed by the three-point bending.

In the phase field simulations, the total energy arises from thermodynamic bulk energy, interfacial energy and strain energy. The thermodynamic energy is represented by a double-well potential; the relative depth of the minima is shifted to represent effects of temperature. The interfacial energy, isotropic here, is obtained by gradient terms which are non-zero in the transition regions. The phase field evolves according to Cahn–Allen dynamics for non-conserved order parameters, and is solved on a two-dimensional grid using finite differences that are second-order accurate in space and first-order accurate in time. A simple relaxation (Gauss–Seidel) method is implemented to find the displacement fields, strain, and stress by solving the equations of mechanical equilibrium with fixed displacement boundary conditions. The system considered corresponds to a beam of length 5 μm and width 1 μm, which is bent so that the strain on the upper and lower edge is 0.5% and −0.5%, respectively.

Received 25 June 2009; accepted 12 August 2009;
published online 13 September 2009

References

1. Cox, P. A. (ed.) *Transition Metal Oxides: An Introduction to Their Electronic Structure and Properties* (Oxford Univ. Press, 1992).
2. Dagotto, E. (ed.) *Nanoscale Phase Separation and Colossal Magnetoresistance* (Springer, 2002).
3. Spaldin, N. A. & Fiebig, M. The renaissance of magnetoelectric multiferroics. *Science* **309,** 391–392 (2005).
4. Choi, K. J. *et al.* Enhancement of ferroelectricity in strained $BaTiO_3$ thin films. *Science* **306,** 1005–1009 (2004).
5. Haeni, J. H. *et al.* Room-temperature ferroelectricity in strained $SrTiO_3$. *Nature* **430,** 758–761 (2004).
6. Wang, J. *et al.* Epitaxial $BiFeO_3$ multiferroic thin film heterostructures. *Science* **299,** 1719–1722 (2003).
7. Locquet, J. P. *et al.* Doubling the critical temperature of $La_{1.9}Sr_{0.1}CuO_4$ using epitaxial strain. *Nature* **394,** 453–456 (1998).
8. Eyert, V. The metal–insulator transitions of VO_2: a band theoretical approach. *Ann. Phys.* **11,** 650–704 (2002).
9. Marezio, M., McWhan, D. B., Remeika, J. P. & Dernier, P. D. Structural aspects of the metal–insulator transitions in Cr-doped VO_2. *Phys. Rev. B* **5,** 2541–2551 (1972).
10. Rakotoniaina, J. C. *et al.* The thermochromic vanadium dioxide: I. Role of stresses and substitution on switching properties. *J. Solid State Chem.* **103,** 81–94 (1993).
11. Biermann, S., Poteryaev, A., Lichtenstein, A. I. & Georges, A. Dynamical singlets and correlation-assisted Peierls transition in VO_2. *Phys. Rev. Lett.* **94,** 026404 (2005).
12. Cavalleri, A., Rini, M. & Schoenlein, R. W. Ultra-broadband femtosecond measurements of the photo-induced phase transition in VO_2: from the mid-IR to the hard X-rays. *J. Phys. Soc. Jpn* **75,** 011004 (2006).
13. Wentzcovitch, R. M., Schulz, W. W. & Allen, P. B. VO_2: Peierls or Mott–Hubbard? A view from band theory. *Phys. Rev. Lett.* **72,** 3389–3392 (1994).
14. Ladd, L. A. & Paul, W. Optical and transport properties of high quality crystals of V_2O_4 near the metallic transition temperature. *Solid State Commun.* **7,** 425–428 (1969).
15. Gu, Q., Falk, A., Wu, J., Ouyang, L. & Park, H. Current-driven phase oscillation and domain-wall propagation in $W_xV_{1-x}O_2$ nanobeams. *Nano Lett.* **7,** 363–366 (2007).
16. Wu, J. *et al.* Strain-induced self organization of metal–insulator domains in single-crystalline VO_2 nanobeams. *Nano Lett.* **6,** 2313–2317 (2006).
17. Wei, J., Wang, Z., Chen, W. & Cobden, D. H. New aspects of the metal–insulator transition in single-domain vanadium dioxide nanobeams. *Nature Nanotech.* **4,** 420–424 (2009).
18. Roytburd, A. L. Thermodynamics of polydomain heterostructures. II. Effect of microstresses. *J. Appl. Phys.* **83,** 239–245 (1998).
19. Tsai, K.-Y., Chin, T.-S. & Shieh, H.-P. D. Effect of grain curvature on nano-indentation measurements of thin films. *Jpn J. Appl. Phys.* **43,** 6268–6273 (2004).
20. Berglund, C. N. & Guggenheim, H. J. Electronic properties of VO_2 near the semiconductor–metal transition. *Phys. Rev.* **185,** 1022–1033 (1969).
21. Cook, O. A. High-temperature heat contents of V_2O_3, V_2O_4 and V_2O_5. *J. Am. Chem. Soc.* **69,** 331–333 (1964).
22. Zhou, J. *et al.* Flexible piezotronic strain sensor. *Nano Lett.* **8,** 3035–3040 (2008).
23. Strelcov, E., Lilach, Y. & Kolmakov, A. Gas sensor based on metal–insulator transition in VO_2 nanowire thermistor. *Nano Lett.* **9,** 2322–2326 (2009).
24. Khachaturyan, A. G. ed. *Theory of Structural Transformation in Solids* (John Wiley, 1983).
25. Qazilbash, M. M. *et al.* Mott transition in VO_2 revealed by infrared spectroscopy and nano-imaging. *Science* **318,** 1750–1753 (2007).
26. Ahn, K. H., Lookman, T. & Bishop, A. R. Strain-induced metal–insulator phase coexistence in perovskite manganites. *Nature* **428,** 401–404 (2004).

27. Burgy, J., Moreo, A. & Dagotto, E. Relevance of cooperative lattice effects and stress fields in phase-separation theories for CMR manganites. *Phys. Rev. Lett.* **92,** 097202 (2004).
28. Dagotto, E. Complexity in strongly correlated electronic systems. *Science* **309,** 257–262 (2005).
29. Dagotto, E. Open questions in CMR manganites, relevance of clustered states and analogies with other compounds including the cuprates. *New J. Phys.* **7,** 67 (2005).
30. Faeth, M. *et al.* Spatially inhomogeneous metal–insulator transition in doped manganites. *Science* **285,** 1540–1542 (1999).
31. Moreo, A., Yunoki, S. & Dagotto, E. Phase separation scenario for manganese oxides and related materials. *Science* **283,** 2034–2040 (1999).
32. Shenoy, V. B., Sarma, D. D. & Rao, C. N. R. Electronic phase separation in correlated oxides: the phenomenon, its present status and future prospects. *ChemPhysChem.* **7,** 2053–2059 (2006).
33. Lee, J. *et al.* Interplay of electron-lattice interactions and superconductivity in $Bi_2Sr_2CaCu_2O_{8+\delta}$. *Nature* **442,** 546–550 (2006).
34. Guiton, B. S., Gu, Q., Prieto, A. L., Gudiksen, M. S. & Park, H. Single-crystalline vanadium dioxide nanowires with rectangular cross sections. *J. Am. Chem. Soc.* **127,** 498–499 (2005).

Acknowledgements

This work was supported in part by the National Science Foundation (grant no. EEC-0425914) and in part by the Laboratory Directed Research and Development Program of Lawrence Berkeley National Laboratory (LBNL; Department of Energy contract no. DE-AC02-05CH11231). Portions of this work were performed at the Molecular Foundry and the National Centre for Electron Microscopy, both at LBNL. J.C.G. and E.E. acknowledge funding by the Focus Center Research Program on Materials, Structures and Devices (FCRP/MSD).

Author contributions

J.W. and J.C. conceived and planned the experiments. J.C. performed the experiments with assistance from W.F. E.E., V.S. and J.C.G. carried out the modelling. H.Z. performed the TEM. S.H., J.W.L.Y., D.R.K. and D.F.O. contributed to materials synthesis and analysis. J.C. and J.W. analysed the data and wrote the paper.

Additional information

Supplementary information accompanies this paper at www.nature.com/naturenanotechnology. Reprints and permission information is available online at http://npg.nature.com/reprintsandpermissions/. Correspondence and requests for materials should be addressed to J.W.

nature nanotechnology

SUPPLEMENTARY INFORMATION

DOI: 10.1038/NNANO.2009.266

J. Cao,[1, 2] E. Ertekin,[3] V. Srinivasan,[3] S. Huang,[1] W. Fan,[1, 4] H. Zheng,[2,5] J. W. L. Yim,[1, 2] D. R. Khanal,[1, 2] D. F. Ogletree,[2,6] J. C. Grossman,[3] and J. Wu[1, 2,3] *

[1]Department of Materials Science and Engineering, University of California, Berkeley, Berkeley, CA 94720, USA

[2]Materials Sciences Division, Lawrence Berkeley National Laboratory, Berkeley, CA 94720, USA

[3]Berkeley Nanosciences and Nanoengineering Institute, University of California, Berkeley, Berkeley, CA 94720, USA

[4]Department of Thermal Science and Energy Engineering, University of Science and Technology of China, Hefei, China

[5]National Center for Electron Microcopy, Lawrence Berkeley National Laboratory, Berkeley, CA 94720, USA

[6]Molecular Foundry, Lawrence Berkeley National Laboratory, Berkeley, CA 94720, USA

*To whom correspondence should be addressed. Email: wuj@berkeley.edu

Synthesis and characterization of VO_2 beams: The VO_2 beams were synthesized using a modified version of the vapor transport method reported previously by Guiton et al[1]. Bulk VO_2 powder was placed in a quartz boat in the center of a horizontal tube furnace. The reaction product was collected on a Si substrate with a thermally grown surface oxide (100 nm and 500 nm) or on quartz substrates downstream from the source boat. The growth was carried out at different conditions including: temperature 900, 950, and 1000 ºC, Ar carrier gas flow rate 4, 10 and 20 sccm, pressure ~ 10 torr, evaporation time ~ 4 hours. The size distribution, lattice structure and crystal orientation of these beams were characterized by scanning electron microscopy, transmission electron microscopy and selected area electron diffraction.

Optical and electrical measurements: Bright-field optical images were recorded using an optical microscope (Leica DM 4000M) equipped with a color CCD camera. Beams with various sizes show optical contrast between the low-temperature, insulating phase and the high-temperature, metallic phases. The sample temperature was controlled by a heater and a resistive temperature sensor. Four-point probe devices were fabricated via photolithography on quartz substrate. The contact electrodes were deposited by sputtering Titanium layer (20 nm) followed by a gold layer (200 nm) onto the lithographically defined pattern. The *in situ* bending of the VO_2 beam in Video S1 was achieved by clamping a VO_2 beam across a gap between two Si chips glued onto a piezoelectric stack, so as to modulate the gap size and stress the VO_2 beam. It can be seen that in the initial state, the beam was in I phase. When uniaxially compressed, a single M-domain formed along the length. Upon further stressing, the beam buckled and an array of triangular I domains showed up parting the curved regions of the beam. The beam reversibly returned to the initial purely I state when the stress was released.

DOI: 10.1038/NNANO.2009.266

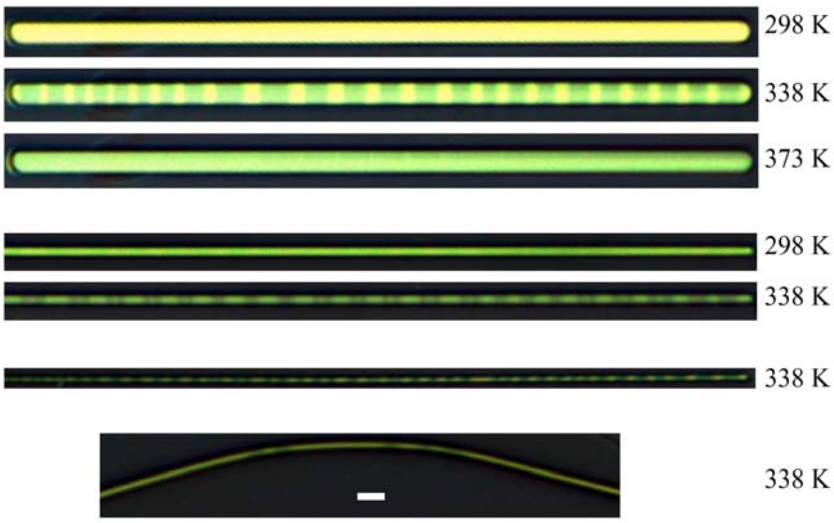

Figure S1 Bright field reflected white-light optical images of VO_2 beams. The beams are in the pure insulating phase (bright contrast) at low temperatures (298 K), pure metallic phase (dark contrast) at high temperatures (373 K), and mixed insulating-metallic domains at intermediate temperatures (338 K). The last image is for a bent, non-clamped beam, while the rest are for beams bottom clamped on a SiO_2 substrate. The scale bar is 2 μm.

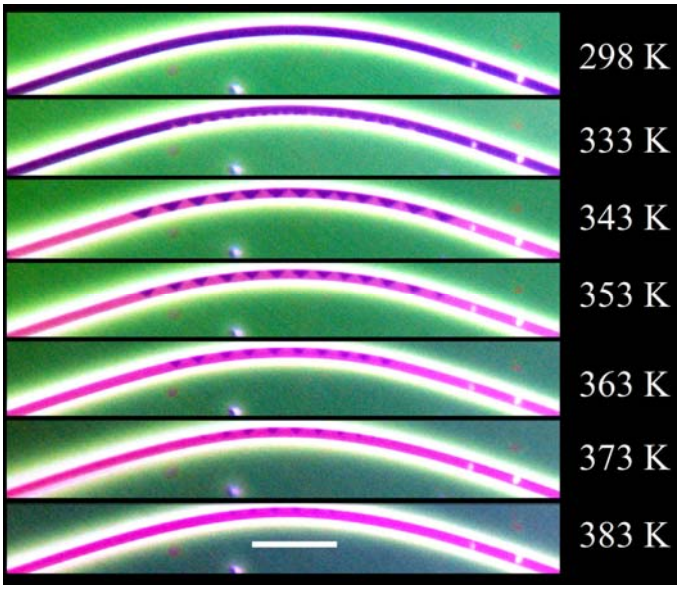

Figure S2 Colour inverted image of Fig. 2a in the main text, showing an array of triangle M-I domains nucleated and co-stabilized by tensile and compressive strain during heating. Bright is M phase and dark is I phase. The scale bar is 10 μm.

Video S1. In situ optical imaging of compressing and then bending a VO_2 beam (width ~1.5 μm, temperature 338 K) showing the creation and elimination of M domains along the beam.

Video S2. Phase field modelling of domain formation in a bent VO_2 beam. This video shows the nucleation and evolution of a periodic array of triangular M and I domains out of a randomly distributed initial state. The system considered corresponds to a beam of length 5 μm and width 1 μm, which is bent so that the initial strain varies linearly from 0.5% at the lower edge to -0.5% at the upper edge. The yellow and dark green colours represent I and M phase, respectively.

Video S3. Phase field modelling of domain formation in a bent VO_2 beam. This video shows the evolution of the strain field. The yellow and dark green colours denote the maximum tensile and maximum compressive strain, respectively.

Video S4. Phase field modelling of domain formation in a bent VO_2 beam. This video shows the evolution of the strain energy density. The yellow and dark green colours denote the highest and lowest strain energy density, respectively.

References

1. Guiton, B.S., Gu, Q., Prieto, A.L., Gudiksen, M.S., & Park, H., Single-Crystalline Vanadium Dioxide Nanowires with Rectangular Cross Sections. *J. Am. Chem. Soc.* **127** (2), 498-499 (2005).